Nonlinear Interference and Unidirectional Wave Mixing in Metamaterials

Alec Rose, Da Huang, and David R. Smith

Center for Metamaterials and Integrated Plasmonics, Duke University, Durham, North Carolina 27708, USA

(Received 19 October 2012; published 5 February 2013)

When both electric and magnetic mechanisms contribute to a particular nonlinear optical process, there exists the possibility for nonlinear interference, often characterized by constructive or destructive interference in the radiation pattern of harmonics and mix waves. However, observation of a significant effect from nonlinear interference requires careful balancing of the various contributions. For this purpose, we propose an artificial metamaterial, using the formalism of nonlinear magnetoelectric coupling to simultaneously engineer the nonlinear polarization and magnetization. We confirm our predictions of nonlinear interference with both simulations and experiment, demonstrating unidirectional wave mixing in two microwave metamaterials. Our results point toward an ever wider range of nonlinear properties, in which nonlinear interference is just one of many potential applications.

DOI: 10.1103/PhysRevLett.110.063901 PACS numbers: 42.65.An, 75.85.+t, 78.67.Pt, 81.05.Xj

Nonlinear optical effects with a magnetic origin can have very different properties compared to those with electric origin. When mechanisms of *both* electric and magnetic natures are present, a particular nonlinear process, such as second-harmonic generation (SHG), can contain multiple contributions with varied strengths and phases, giving rise to constructive and destructive interference. In natural materials, this so-called nonlinear interference has provided a pathway for observing antiferromagnetic domains [1–6], since the antiferromagnetic properties, and in turn the nonlinear interference effects, reverse themselves in neighboring domains.

In terms of three-wave mixing, the various dipolar contributions are manifest in eight nonlinear susceptibility tensors, defined through the second-order polarization and second-order magnetization,

$$\begin{aligned}\vec{P}^{(2)}(\omega_s) = \sum_{(qr)} [&\bar{\bar{\chi}}^{(2)}_{eee}(\omega_s;\omega_q,\omega_r)\vec{E}(\omega_q)\vec{E}(\omega_r) \\ &+ \bar{\bar{\chi}}^{(2)}_{emm}(\omega_s;\omega_q,\omega_r)\vec{H}(\omega_q)\vec{H}(\omega_r) \\ &+ \bar{\bar{\chi}}^{(2)}_{eem}(\omega_s;\omega_q,\omega_r)\vec{E}(\omega_q)\vec{H}(\omega_r) \\ &+ \bar{\bar{\chi}}^{(2)}_{eme}(\omega_s;\omega_q,\omega_r)\vec{H}(\omega_q)\vec{E}(\omega_r)], \quad (1)\end{aligned}$$

$$\begin{aligned}\mu_0\vec{M}^{(2)}(\omega_s) = \sum_{(qr)} [&\bar{\bar{\chi}}^{(2)}_{mmm}(\omega_s;\omega_q,\omega_r)\vec{H}(\omega_q)\vec{H}(\omega_r) \\ &+ \bar{\bar{\chi}}^{(2)}_{mee}(\omega_s;\omega_q,\omega_r)\vec{E}(\omega_q)\vec{E}(\omega_r) \\ &+ \bar{\bar{\chi}}^{(2)}_{mme}(\omega_s;\omega_q,\omega_r)\vec{H}(\omega_q)\vec{E}(\omega_r) \\ &+ \bar{\bar{\chi}}^{(2)}_{mem}(\omega_s;\omega_q,\omega_r)\vec{E}(\omega_q)\vec{H}(\omega_r)], \quad (2)\end{aligned}$$

respectively, where $\omega_s = \omega_q + \omega_r$ is the frequency of the nonlinear response, $\omega_{q,r}$ are the frequencies of the driving fields, and $\bar{\bar{\chi}}^{(2)}$ represent the various second-order susceptibility tensors. While the first terms in both expressions represent pure electric and magnetic nonlinearities, respectively, the other six involve the mixing of electric and magnetic responses and fields, or so-called nonlinear magnetoelectric coupling. For example, Fiebig *et al.* exploited the similar magnitudes of $\chi^{(2)}_{eee}$ and $\chi^{(2)}_{mee}$ in Cr_2O_3 to experimentally observe nonlinear interference via SHG [1,2]. However, natural materials suffer from (typically) weak magnetic contributions, limiting the overall efficiency of nonlinear interference and nonlinear magnetoelectric coupling in general.

Alternatively, certain plasmonic nanoparticles have shown promise in supporting strong effective magnetic and quadrupolar contributions [7–11], which has led to the observation of nonlinear interference in the generation of optical harmonics [12–14]. In particular, Zdanowicz *et al.* attributed asymmetric SHG from *L*-shaped gold nanoparticles to the nonlinear interference between second-order electric, magnetoelectric, and quadrupolar tensors [15]. This recent progress suggests that artificial media, or metamaterials, constructed from arrays of nanoparticles might provide a means to *tailor* the effective nonlinear susceptibilities.

Indeed, clever structuring of metamaterials can lead to effective magnetic and magnetoelectric behavior, even when composed of nonmagnetic materials [16]. This flexibility in the linear behavior of metamaterials has lead to such exciting phenomena as negative refraction [17] and electromagnetic cloaking [18]. The split-ring resonator (SRR), for example, is the canonical magnetic metamaterial [16], wherein an intrinsic resonance is formed by inserting a capacitive gap into a conducting loop. The SRR's resonance is typically excited by incident magnetic fields that couple inductively to the structure. When these same metamaterials are hybridized with nonlinear components, the degrees of freedom grow exponentially. This sort of control and balance of nonlinear properties is paramount to a whole host of phenomena. In this context, nonlinear

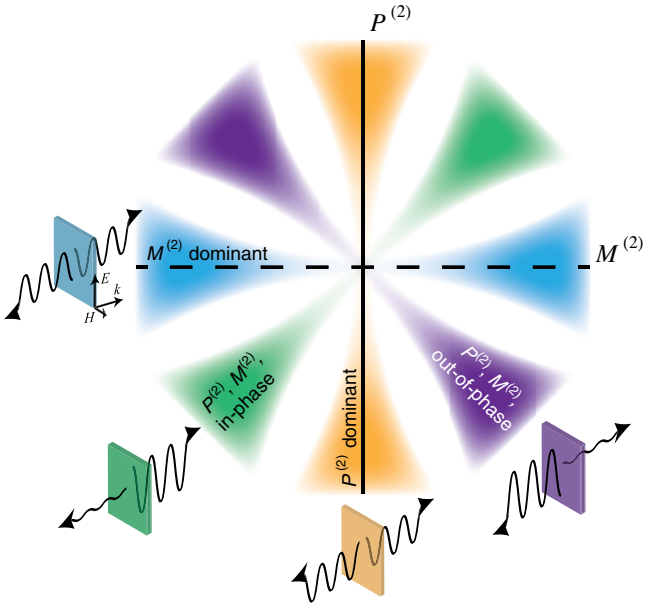

FIG. 1 (color online). Graphical illustration of the nonlinear parameter space. The insets depict nonlinear generation (arrows indicate electric fields) from a thin nonlinear slab for four limiting cases, corresponding to the areas under the colored cones. When the second-order polarization (magnetization) is dominant, as in the vertical (horizontal) cones, the nonlinear generation resembles an electric (magnetic) dipole. When a second-order polarization *and* magnetization are present, however, the interference can favor nonlinear generation in a particular direction, illustrated by the insets next to the diagonal cones. This is an oversimplification, however, as both the polarization and magnetization are, in general, complex valued.

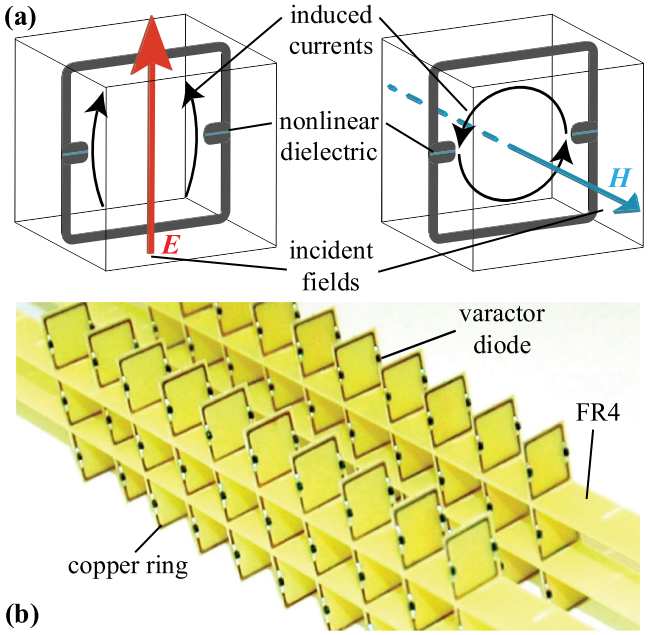

FIG. 2 (color online). (a) The nonlinear SRR proposed in Ref. [19] for observation of nonlinear interference. Both electric (left) and magnetic (right) incident fields interact with the nonlinear dielectric, resulting in nonlinear magnetoelectric coupling. (b) Photograph of the analogous VLSRRs from Ref. [27].

interference is seen to occupy a region in the more general nonlinear parameter space, depicted in Fig. 1, in which careful balance of the nonlinear polarization and magnetization leads to unidirectional harmonic and mix-wave generation. Nonlinear magnetoelectric coupling, in turn, offers a platform for accessing the full range of nonlinear properties and phenomena [19].

Quasianalytic expressions for the effective magnetoelectric nonlinear properties of metamaterials have been derived generally via a Bloch mode analysis, assuming only electric nonlinearities [19]. Qualitatively, a general requirement for nonlinear magnetoelectric coupling is for the fields locally induced by incident electric and magnetic fields to overlap within the nonlinear element. A SRR design, consisting of a metallic ring with two nonlinear dielectric-loaded gaps, was proposed for the observation of nonlinear interference, as shown in Fig. 2(a). Although ultimately intended for operation at terahertz or infrared frequencies, microwave metamaterials offer a convenient platform for proof-of-concept demonstrations. When placed in the capacitive gaps, the field-dependent properties of varactor diodes have allowed the varactor-loaded (VL) SRR to be used as a microwave nonlinear metamaterial [20–23], leading to proof-of-concept demonstrations of resonance tuning [23,24], solitons [25], and negative-index SHG [26], to name a few.

In this Letter, we employ a microwave nonlinear magnetoelectric SRR, consisting of dual-gap copper rings on an FR4 grade printed circuit board substrate, loading both capacitive gaps with Skyworks SMV1231 varactor diodes [27] [see Fig. 2(b)]. These VLSRRs are then divided into two groups, differing only in the relative orientation of the varactor diodes: symmetric (varactors oriented together) and antisymmetric (varactors oriented oppositely), as shown in Fig. 3. The relative orientation of the varactors plays a key role in the VLSRR's nonlinear properties and, thus, nonlinear interference effects. The qualitative features of the second-order susceptibilities in both VLSRR samples are obtained from a Bloch mode analysis [19], which are used together with a simple one-dimensional model to predict the nonlinear behavior of a thin slab. We then study difference frequency generation (DFG) in these VLSRRs, confirming the presence of nonlinear interference in a single layer by experiment and simulation.

To describe nonlinear interference in the VLSRRs, we consider the interaction between two waves, termed signal (s) and pump (p), in producing idler (i) waves via DFG, such that $\omega_i = \omega_p - \omega_s$, where ω is an angular frequency. For a simple one-dimensional system, the forward ($+$) and backward ($-$) idler waves satisfy the scalar wave equation [19]

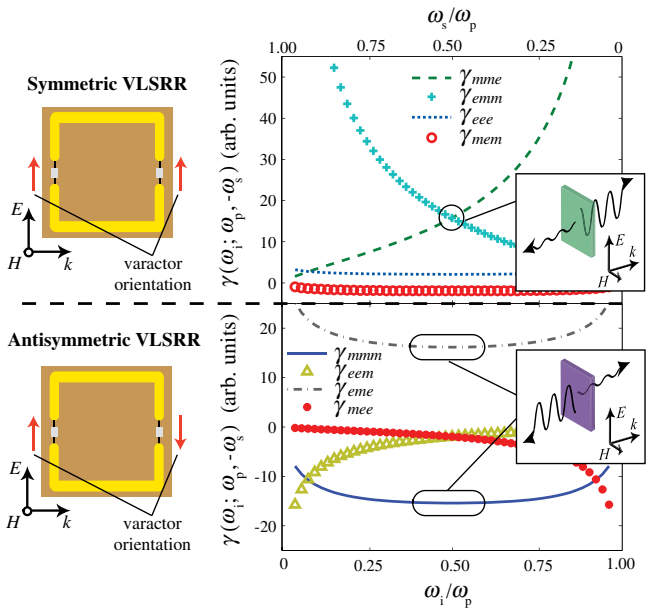

FIG. 3 (color online). Second-order susceptibilities calculated for symmetric and antisymmetric nonlinear SRRs in Ref. [19] as a function of $\omega_i/\omega_p = 1 - \omega_s/\omega_p$, for ω_p fixed at the SRR resonance. The resonant susceptibilities (involving the magnetic component of the pump field) are dominant over most of the spectrum in each VLSRR, so that DFG is dominated by their interference, as in Eqs. (6) and (8). The insets graphically illustrate the resulting nonlinear interference in each sample, with the optimum occurring in the neighborhood of $\omega_s \approx \omega_i \approx \omega_p/2$.

$$\frac{\partial A_i^{\pm}}{\partial z} = S^{\pm} e^{\mp i k_i z}, \tag{3}$$

where we have defined the wave amplitudes $A^{\pm}$ such that the wave intensity is $I^{\pm} = 2|A^{\pm}|^2$. The pump and signal waves mix in the nonlinear medium to produce source terms at the difference frequency, given by

$$S^{\pm} = \pm i \frac{\omega_i}{2}\left[\sqrt{Z_i} P^{(2)}(\omega_i) \pm \frac{1}{\sqrt{Z_i}} \mu_0 M^{(2)}(\omega_i)\right], \tag{4}$$

where Z_i is the wave impedance at ω_i and $P^{(2)}(\omega_i)$ and $M^{(2)}(\omega_i)$ are given by Eqs. (1) and (2).

To simplify the analysis, we fix the pump wave at the magnetic resonance. Since the electric field of the pump wave cannot excite the VLSRR's magnetic resonance, we can neglect all nonresonant nonlinearities. Moreover, the internal symmetry of the symmetric VLSRR suppresses all axial second-order tensors [19], such that $\chi^{(2)}_{mmm} = \chi^{(2)}_{mee} = \chi^{(2)}_{eme} = \chi^{(2)}_{eem} = 0$. Thus, the source term for the symmetric VLSRR reduces to just

$$S^{\pm} = \pm i\omega_i\left[\sqrt{Z_i}\chi^{(2)}_{emm}(\omega_i;\omega_p,-\omega_s)H(\omega_p)H(\omega_s)^* \pm \frac{1}{\sqrt{Z_i}}\chi^{(2)}_{mme}(\omega_i;\omega_p,-\omega_s)H(\omega_p)E(\omega_s)^*\right]. \tag{5}$$

For an optically thin slab of extent a, we can neglect phase matching and pump depletion, so that Eq. (3) has the simple solution

$$I_i^{\pm} = \frac{1}{2} a^2 I_p I_s |\gamma_{emm} \pm \gamma_{mme}|^2, \tag{6}$$

where the coupling coefficients γ are just renormalizations of the nonlinear susceptibilities,

$$\gamma_{g_i g_p g_s} = \omega_i \sqrt{G_i G_p G_s}\chi^{(2)}_{g_i g_p g_s}, \tag{7}$$

where $G_i = Z_i$ for $g_i = e$, $G_i = 1/Z_i$ for $g_i = m$, and likewise for the pump and signal. For compactness, we have dropped the explicit frequency dependence. Thus, we expect to observe maximum nonlinear interference, i.e., maximum asymmetry between the forward and backward idler intensities, when the magnitudes of $\gamma_{mme}(\omega_i;\omega_p,-\omega_s)$ and $\gamma_{emm}(\omega_i;\omega_p,-\omega_s)$ are roughly equal. We can infer the frequency range for maximum nonlinear interference from the permutation symmetries, noting that simultaneously interchanging the first and last frequencies and field components should leave the nonlinearity unchanged, such that $\gamma_{mme}(\omega_i;\omega_p,-\omega_s) = \gamma_{emm}(\omega_s;\omega_p,-\omega_i)$ [19]. It follows that $\gamma_{emm}(\omega_i;\omega_p,-\omega_s)$ and $\gamma_{mme}(\omega_i;\omega_p,-\omega_s)$ are equal at the degeneracy point, $\omega_s = \omega_i$, denoted by the black circle in Fig. 3. Thus, for $\omega_s \approx \omega_i \approx \omega_p/2$, Eq. (6) implies constructive (destructive) interference for the forward (backward) propagating idler.

We can follow the same procedure for the antisymmetric VLSRR, noting that the internal symmetries suppress all *polar* second-order tensors, such that $\chi^{(2)}_{eee} = \chi^{(2)}_{mme} = \chi^{(2)}_{mem} = \chi^{(2)}_{emm} = 0$. Thus, the idler waves emitted by a thin slab are given by

$$I_i^{\pm} = \frac{1}{2} a^2 I_p I_s |\gamma_{eme} \pm \gamma_{mmm}|^2. \tag{8}$$

The dominant nonlinearities contributing to DFG in the antisymmetric VLSRR are $\gamma_{eme}(\omega_i;\omega_p,-\omega_s)$ and $\gamma_{mmm}(\omega_i;\omega_p,-\omega_s)$, and so we cannot rely on permutation symmetry. Instead, we use the fact that, in the frequency range of interest, the VLSRR couples nonresonantly to the electric field and resonantly to the magnetic field. Since induction vanishes at sufficiently low frequencies, this implies a frequency range where the VLSRR's coupling to electric and magnetic fields are comparable. We have purposefully designed this VLSRR to support roughly balanced electric and magnetic coupling for $\omega_s \approx \omega_i \approx \omega_p/2$, so that nonlinear interference in the two samples can be directly compared. However, in contrast to the symmetric VLSRR, Fig. 3 shows that the antisymmetric VLSRR's dominant nonlinearities are out of phase, i.e., $\gamma_{eme}(\omega_i;\omega_p,-\omega_s) \approx -\gamma_{mmm}(\omega_i;\omega_p,-\omega_s)$ for $\omega_s \approx \omega_i \approx \omega_p/2$, so that, according to Eq. (8), the

antisymmetric VLSRR is expected to favor idler emission in the *backward* direction.

To observe nonlinear interference, the VLSRRs are arranged into square lattices with separation $a = 1$ cm, as in Fig. 2(b), forming a thin one-dimensional layer. The samples are then placed into the impedance-matched transmission line apparatus of Ref. [28], shown schematically in Fig. 4(a). Pump and signal waves are launched from Agilent PNA E8364B and PNA-X N5245A network analyzers, respectively. The pump power is 0 dBm at fixed frequency $\omega_p/2\pi = 970$ MHz, corresponding to the magnetic resonance frequency of the VLSRRs, while the 10 dBm signal has its frequency swept from 400 to 570 MHz. The VLSRRs generate idler waves in both directions via DFG, which are measured at ports 1 and 2 of the network analyzer. The low-pass filter (LPF) and band-pass filter (BPF) block the pump and signal, respectively, minimizing the DFG noise generated by the network analyzers themselves. A 6 dB splitter is used to draw a portion of the forward idler signal for measurement at port 2. Assuming perfect matching at the interconnects, the splitter and attenuator ensure that reflections from the band-pass filter incur at least 26 dB of attenuation before reaching the VLSRRs and/or measurement ports throughout the signal or idler frequency band. Ultimately, this ensures that the directionality of the idler and signal waves is preserved throughout. The forward and backward idler spectra are corrected for attenuation along the paths to their respective ports and displayed in Fig. 4(b). The idler spectra show considerable unidirectionality, with the symmetric VLSRR favoring forward generation by more than 6 times and the antisymmetric VLSRR favoring backward generation by an order of magnitude. As such, the results are fully consistent with the predicted nonlinear interference, mediated by nonlinear magnetoelectric coupling in the VLSRR samples.

To support the experimental data, we also include frequency domain scattering simulations in COMSOL multiphysics, as in Ref. [27]. Pump and signal plane waves are launched at a single unit cell with appropriate periodic boundary conditions, simulating an infinite slab, from which the forward and backward DFG signals are collected, using a Taylor expansion of the varactor's SPICE (Simulation Program with Integrated Circuit Emphasis) model to simulate DFG in the varactors [29]. For direct comparison with experiment, we take into account the attenuation in the experimental setup, as well as the inhomogeneous mode profile within the transmission line. The resulting SH spectra are plotted in Fig. 4(b), in quantitative agreement with measured data. While contributions from the nonresonant nonlinearities are expected to prohibit perfect unidirectionality, it is likely that some amount of the weak measured spectra are attributable to unwanted reflections in the experimental setup, implying that the unidirectionality of the fabricated VLSRRs may approach the ideal values achieved in simulation for improved setups.

Both the analysis provided here and the general SRR designs and properties are scalable to terahertz and infrared frequencies, simply by replacing the varactors with nonlinear crystals or placing the entire structure on a nonlinear substrate. While the configuration of the antisymmetric SRR represents a difficult fabrication challenge, it is easy to envision implementing the symmetric SRR via lithography over gallium arsenide (GaAs), for example, as in Ref. [10] for near-infrared frequencies and in Ref. [30] for terahertz. Moreover, there exist a number of metamaterial structures capable of supporting a similar overlap of the electrically and magnetically driven local fields, such as paired nanorods and fishnet structures [31]. By proper inclusion of nonlinear dielectrics in these metamaterials,

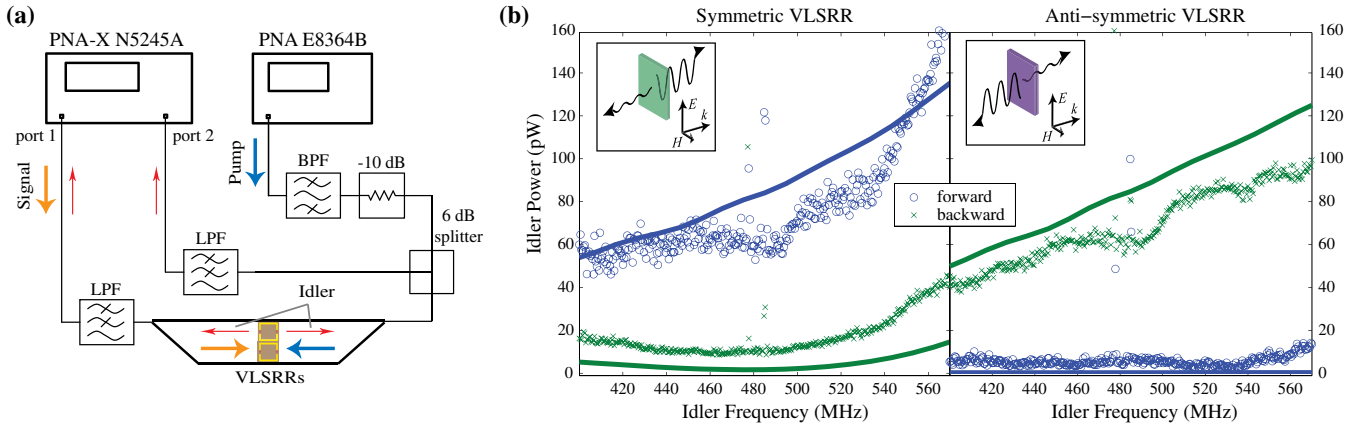

FIG. 4 (color online). BPF (a) Schematic of the experimental setup for measuring DFG. (b) Plots of the forward and backward experimental DFG spectra generated by the symmetric VLSRRs (left) and the antisymmetric VLSRRs (right). The unidirectionality of the spectra confirm the presence of strong nonlinear interference, as illustrated in the insets. The solid lines show the results of simulations for comparison.

effective properties throughout the nonlinear parameter space should be possible at terahertz, infrared, and even visible frequencies.

This work was supported by the Air Force Office of Scientific Research (Contract No. FA9550-09-1-0562). We thank Daniel Gauthier for access to equipment and helpful discussions.

[1] M. Fiebig, D. Fröhlich, B. B. Krichevtsov, and R. V. Pisarev, Phys. Rev. Lett. **73**, 2127 (1994).
[2] M. Fiebig, D. Fröhlich, G. Sluyterman, and R. V. Pisarev, Appl. Phys. Lett. **66**, 2906 (1995).
[3] Y. Tanabe, M. Fiebig, and E. Hanamura, in *Magneto-optics*, edited by S. Sugano and N. Kojima (Springer, New York, 2000).
[4] M. Fiebig, T. Lottermoser, D. Frohlich, A. V. Goltsev, and R. V. Pisarev, Nature (London) **419**, 818 (2002).
[5] M. Fiebig, V. V. Pavlov, and R. V. Pisarev, J. Opt. Soc. Am. B **22**, 96 (2005).
[6] R. V. D. Sa and C. Gros, Eur. Phys. J. B **14**, 301 (2000).
[7] J. R. Krenn, G. Schider, W. Rechberger, B. Lamprecht, A. Leitner, F. R. Aussenegg, and J. C. Weeber, Appl. Phys. Lett. **77**, 3379 (2000).
[8] K. L. Kelly, E. Coronado, L. L. Zhao, and G. C. Schatz, J. Phys. Chem. B **107**, 668 (2003).
[9] M. W. Klein, C. Enkrich, M. Wegener, and S. Linden, Science **313**, 502 (2006).
[10] F. B. P. Niesler, N. Feth, S. Linden, J. Niegemann, J. Gieseler, K. Busch, and M. Wegener, Opt. Lett. **34**, 1997 (2009).
[11] J. Petschulat, A. Chipouline, A. Tünnermann, T. Pertsch, C. Menzel, C. Rockstuhl, and F. Lederer, Phys. Rev. A **80**, 063828 (2009).
[12] S. Kujala, B. K. Canfield, M. Kauranen, Y. Svirko, and J. Turunen, Phys. Rev. Lett. **98**, 167403 (2007).
[13] J. Butet, J. Duboisset, G. Bachelier, I. Russier-Antoine, E. Benichou, C. Jonin, and P.-F. Brevet, Nano Lett. **10**, 1717 (2010).
[14] M. Chandra, A.-M. Dowgiallo, and K. L. Knappenberger, J. Am. Chem. Soc. **134**, 4477 (2012).
[15] M. Zdanowicz, S. Kujala, H. Husu, and M. Kauranen, New J. Phys. **13**, 023025 (2011).
[16] J. B. Pendry, A. J. Holden, D. J. Robbins, and W. J. Stewart, IEEE Trans. Microwave Theory Tech. **47**, 2075 (1999).
[17] R. A. Shelby, D. R. Smith, and S. Schultz, Science **292**, 77 (2001).
[18] D. Schurig, J. J. Mock, B. J. Justice, S. A. Cummer, J. B. Pendry, A. F. Starr, and D. R. Smith, Science **314**, 977 (2006).
[19] A. Rose, S. Larouche, E. Poutrina, and D. R. Smith, Phys. Rev. A **86**, 033816 (2012).
[20] M. Lapine, M. Gorkunov, and K. H. Ringhofer, Phys. Rev. E **67**, 065601 (2003).
[21] A. A. Zharov, I. V. Shadrivov, and Y. S. Kivshar, Phys. Rev. Lett. **91**, 037401 (2003).
[22] I. V. Shadrivov, A. A. Zharov, and Y. S. Kivshar, J. Opt. Soc. Am. B **23**, 529 (2006).
[23] B. Wang, J. Zhou, T. Koschny, and C. M. Soukoulis, Opt. Express **16**, 16058 (2008).
[24] I. V. Shadrivov, S. K. Morrison, and Y. S. Kivshar, Opt. Express **14**, 9344 (2006).
[25] L. English, S. Wheeler, Y. Shen, G. Veldes, N. Whitaker, P. Kevrekidis, and D. Frantzeskakis, Phys. Lett. A **375**, 1242 (2011).
[26] A. Rose, D. Huang, and D. R. Smith, Phys. Rev. Lett. **107**, 063902 (2011).
[27] A. Rose, D. Huang, and D. R. Smith, Appl. Phys. Lett. **101**, 051103 (2012).
[28] S. Larouche, A. Rose, E. Poutrina, D. Huang, and D. R. Smith, Appl. Phys. Lett. **97**, 011109 (2010).
[29] E. Poutrina, D. Huang, and D. R. Smith, New J. Phys. **12**, 093010 (2010).
[30] K. Fan, H. Hwang, M. Liu, A. Strikwerda, A. Sternbach, J. Zhang, X. Zhao, X. Zhang, K. Nelson, and R. Averitt, arXiv:1208.1538.
[31] V. M. Shalaev, Nat. Photonics **1**, 41 (2007).